Ocean Dynamics (2009) 59:167–181
DOI 10.1007/s10236-008-0159-0

Temporal and spatial circulation patterns in the East Frisian Wadden Sea

Emil V. Stanev · Sebastian Grayek · Joanna Staneva

Received: 14 May 2008 / Accepted: 18 October 2008 / Published online: 2 December 2008

Abstract This work deals with the analysis of simulations carried out with a primitive equation numerical model for the region of the East Frisian Wadden Sea. The model, with 200-m resolution, is forced by wind, air–sea heat, and water fluxes and river runoff and is nested in a German Bight 1-km-resolution numerical model, the latter providing tidal forcing for the fine resolution model. The analysis of numerical simulations is focused both on responses due to moderate conditions, as well as to extreme events, such as the storm surge Britta, for which the model demonstrates very good skills. The question addressed in this paper is how well the model output can be compressed with the help of empirical orthogonal function analysis. It is demonstrated that, for the short-time periods of the order of a spring–neap cycle, only a few modes are necessary to almost fully represent the circulation. This is just an illustration that the circulation in this region is subject to the dominating tidal forcing, creating clear and relatively simple response patterns. However, for longer periods of about several months, wind forcing is also very important, and correspondingly, the circulation patterns become much more complex. Possible applications of the results in hindcasting and forecasting of hydrodynamics and sediment dynamics in the coastal zone are considered.

Keywords Tidal basins · Statistical characteristics · Predictability of circulation

Responsible Editor: Jörg-Olaf Wolff

E. V. Stanev (✉) · J. Staneva
Institute for Coastal Research, GKSS Research Centre,
Max-Planck-Strasse 1, 21502 Geesthacht, Germany
e-mail: emil.stanev@gkss.de

E. V. Stanev · S. Grayek
Institute for Chemistry and Biology of the Sea,
University of Oldenburg, Carl-von-Ossietzky-Strasse 9-11,
26111 Oldenburg, Germany

1 Introduction

A considerable body of work concerning the response of the coastal ocean to tides based on local observations, tidal gauges data, etc., already exists. However, spatial patterns are much less clear because direct observations over large areas with high spatial resolution are limited. Remote sensing data also do not help much: altimeter data are not precise enough in the near coastal zone and ocean color or AVHRR data are affected by cloud conditions and do not provide complete information with sufficient temporal resolution. In the East Frisian Wadden Sea, which is the area of our research interest, the temporal and spatial variability derived from statistical analyses of outputs from numerical models has not been sufficiently explored, although some initial steps have already been made (Stanev et al. 2007b).

The work presented here has been carried out within the framework of the research programme "BioGeoChemistry of Tidal Flats," which combined various research activities aimed to improve the basic understanding of functioning of these areas, including circulation and sediment transport (Staneva et al. 2008). Our major aim here is to make an initial effort towards developing techniques that would enable the best use of data for state estimates and forecasting purposes.

One necessary step, before going deeper into this issue and before addressing data assimilation, is to understand the dominating statistical properties of coastal dynamics.

The German Bight (Fig. 1a), which is bordered by the coasts of the Netherlands, Germany, and Denmark, is situated in the south-eastern corner of the North Sea. It is well established that the wind in this area results in a cyclonic residual circulation, i.e., a circulation in the direction of propagation of the tidal wave (from west to east along the southern boundary and from south to north along the western coasts of Germany and Denmark).

The East-Frisian Wadden Sea is one of the shallowest areas of the German Bight, being characterized by a series of barrier islands, each 5–10 km long in the east–west direction and 2–3 km wide (Fig. 1b). The tidal range varies from ∼ 2.5 m (Isles of Borkum and Sylt) to ∼ 3.5 m (the Elbe Estuary), i.e., the region is exposed to upper meso-tidal conditions.

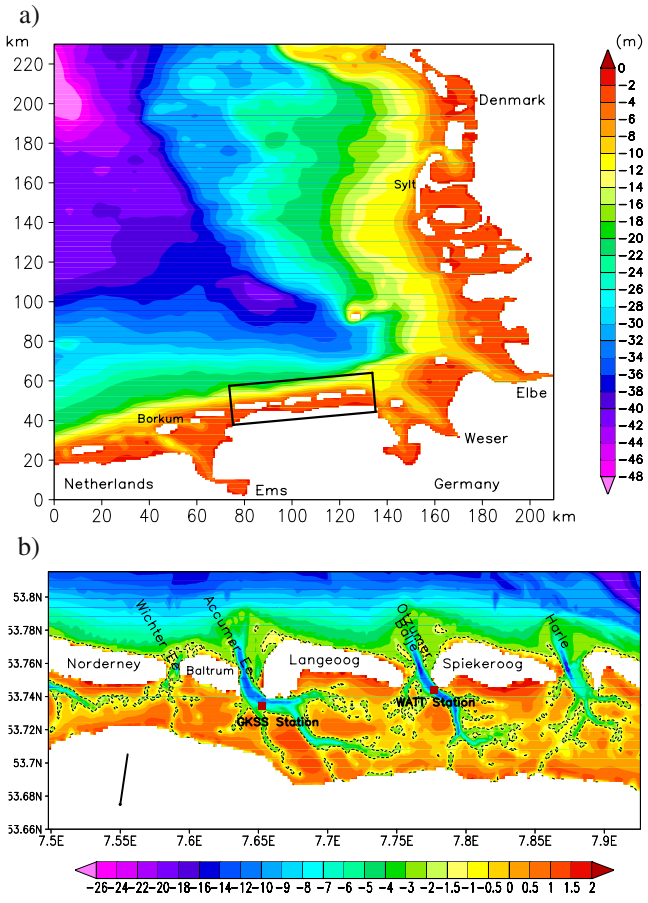

Fig. 1 Topography of the German Bight (**a**) and East Frisian Wadden Sea (**b**). *Dashed line* in **b** contours regions, which are subject to drying. The position of continuously operating data stations are given with *red squares*

Wadden Sea water periodically mixes with North Sea waters (during flooding) and is partially transported into the North Sea (during ebb). In this way, the Wadden Sea acts as a buffer mixing-zone between ocean and land. The exchange of water and properties between the Wadden Sea and the German Bight are known from numerical simulations (Stanev et al. 2003, b, 2007b) and numerous observations (see this special issue).

It is well-known that one fundamental characteristic of the East-Frisian Wadden Sea is the vigorous suspended matter dynamics (Santamarina Cuneo and Flemming 2000; Burchard et al. 2008) triggered by the turbulence due to velocity shear (Stanev et al. 2007a) and wind waves (Gayer et al. 2006; Stanev et al. 2006). Understanding sediment dynamics is, thus, crucially dependent upon the knowledge of the turbulence regime. Therefore, specific attention in this paper is also paid to the question of how complex the turbulence patterns are in the region of the East Frisian Wadden Sea.

Detailed validation of numerical models against observations at fixed locations (Stanev et al. 2003, 2007b), and over larger areas (Staneva et al. 2008) demonstrates a good quality of numerical simulations and motivates us to address the question: what are the dominating temporal and spatial patterns? Provided that the latter show some robustness, we could hope that it would not be too difficult to extend this research towards the issue of predictability, which has never been addressed for this region.

The paper is structured as follows: Section 2 describes the numerical model and setup, Section 3 provides a description of the simulated spatial and temporal patterns, and Section 4 presents the statistical reconstruction of simulations. The paper ends with brief conclusions.

2 Numerical model

The model system used here consists of two models with different horizontal resolution: a German Bight model (GBM) and a Wadden Sea model. Both models are based on the 3-D General Estuarine Transport Model (Burchard and Bolding 2002), in which the equations for the three velocity components u, v, and w; sea-level elevation (SLE) ζ; temperature T; and salinity S, as well as the equations for turbulent kinetic energy (TKE) and the eddy dissipation rate due to viscosity, are solved. The models use terrain-following equidistant vertical coordinates (σ coordinates) and are capable of simulating drying and flooding of tidal flats. The

vertical column is discretized into ten nonintersecting layers. The application of the models to the area of our study is described by Staneva et al. (2007b, 2008), and we refer to these papers for more details.

The Wadden Sea model with a resolution of 200 m is nested in a GBM with a resolution of about 1 km (Staneva et al. 2008). Both models use spherical horizontal grids. The atmospheric forcing for both models is computed through bulk aerodynamic formulas using 6-hourly European Centre for Medium-Range Weather Forecasts (ECMWF) reanalyses data. Below, we briefly formulate the differences in the forcing of the two models.

For the outer mode (GBM), the river run-off for the rivers Elbe, Ems, and Weser is taken from the 1-hourly data provided by the *Bundesamt für Seeschifffahrt und Hydrographie* (BSH). The lateral boundary conditions of sea surface elevations, salinity, and temperature are taken from the operational BSH model (Dick and Sötje 1990; Dick et al. 2001).

For the inner (Wadden Sea) model, the forcing at the open boundaries is taken from the simulations with the GBM (Staneva et al. 2008) and interpolated in time and space onto the grid points along the boundaries of the Wadden Sea regional model. The nesting is one-way, i.e., the nested model receives boundary values from the coarser model but does not influence the coarser resolution model. The fresh-water fluxes from the main tributaries in the region are taken from the observations compiled by Reinke et al. (2000). Initial conditions are set to zero for sea level and velocity. Temperature and salinity are taken from climatology. The experience with the coupled GBM and Wadden Sea model showed that the circulation reaches a quasiperiodic state in only a few tidal cycles.

The present study analyzes numerical simulations carried out for the period September to December 2006. This 4-month period is enough to resolve the dominant temporal scales associated with tidal (flood-ebb, spring–neap) and atmospheric (synoptic) forcing. Compared to earlier modelling studies for the same region based on this model, the present one also demonstrates the response to extreme events. One such event was the storm surge Britta on 1 November 2006. This event extended over the entire North Sea (Fig. 2a, b), atmospheric pressure was below 984 hPa, and extreme values of sea level (Fig. 2c) were reached in many continental locations (e. g. Emden 3.59 m above the mean high water), as well as at barrier islands (Langeoog und Wangerooge). This storm surge belongs to the strongest ones observed in the last 100 years along the Lower Saxony coast. The maximum observed wind speeds on most barrier islands were above 125 km/h

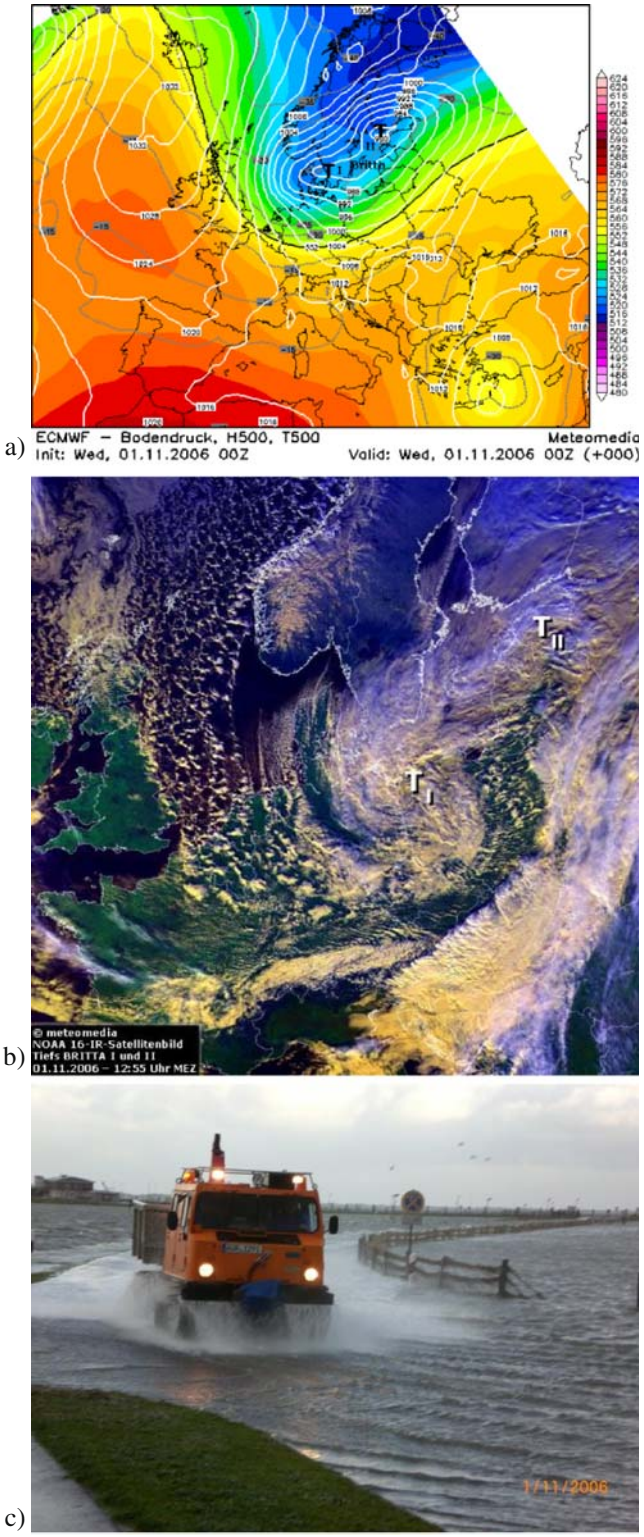

Fig. 2 Surface pressure (**a**), satellite image (**b**), and visual observation (**c**) during storm surge Britta. Courtesy: European Centre for Medium-Range Weather Forecasts (*ECMWF*), National Oceanic and Atmospheric Administration (*NOAA*), and *Niedersächsischer Landesbetrieb für Wasserwirtschaft, Küsten- und Naturschutz* (*NLWKN*), Aurich, Germany

(the estimates based on ECMWF reanalysis data, Fig. 3, give slightly lower values).

The results from our simulations are described in more detail by Staneva et al. (2008). In the present paper, we focus on the circulation (Fig. 4), in particular, as it concerns the transport through the straits. The general pattern is characterized by extreme velocities in the tidal inlets, westward currents in front of the barrier islands during ebb, and eastward currents during flood.

Extremely stormy weather during some periods enabled us to analyze the response of the model in very special conditions. Although Fig. 4b and d correspond to the same tidal phases (shortly after the flood starts, i.e., shortly after low water) during two consequent neap–spring tidal periods, the East-Frisian Wadden Sea does not get dry during the first period (storm Britta). Also noteworthy is the much higher ebb velocity during storm Britta (compare Fig. 4a and c), particularly on the tidal flats.

The comparison with observations (Fig. 5) demonstrates that the model replicates well the major sea-level variability in the area of our simulations. The reason for this good agreement between the Wadden Sea model and the observations needs to be explained. Sea level displays rather homogeneous patterns with very small gradients in the north–south direction (Fig. 4). A more detailed analysis of our simulations demonstrates that the sea level in the Wadden Sea model (a very small coastal area) responds synchronously to external forcing, which is provided by the GBM. This forcing shows almost equal oscillations along the northern model boundary with some phase

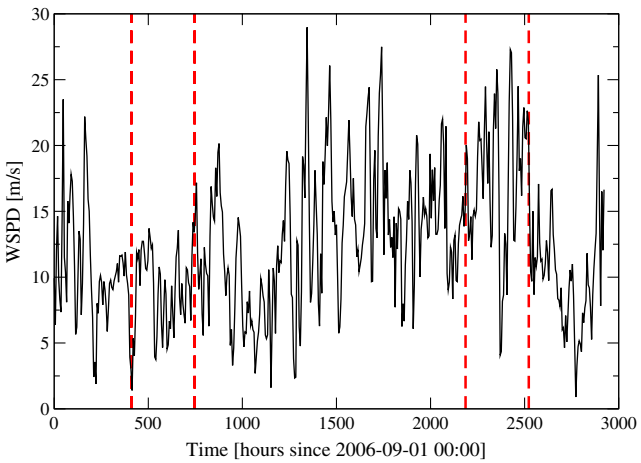

Fig. 3 Mean wind magnitude in the model region during the period of simulations based on ECMWF reanalysis data. The *vertical dashed lines* display the two analysis periods, "calm" and "windy"

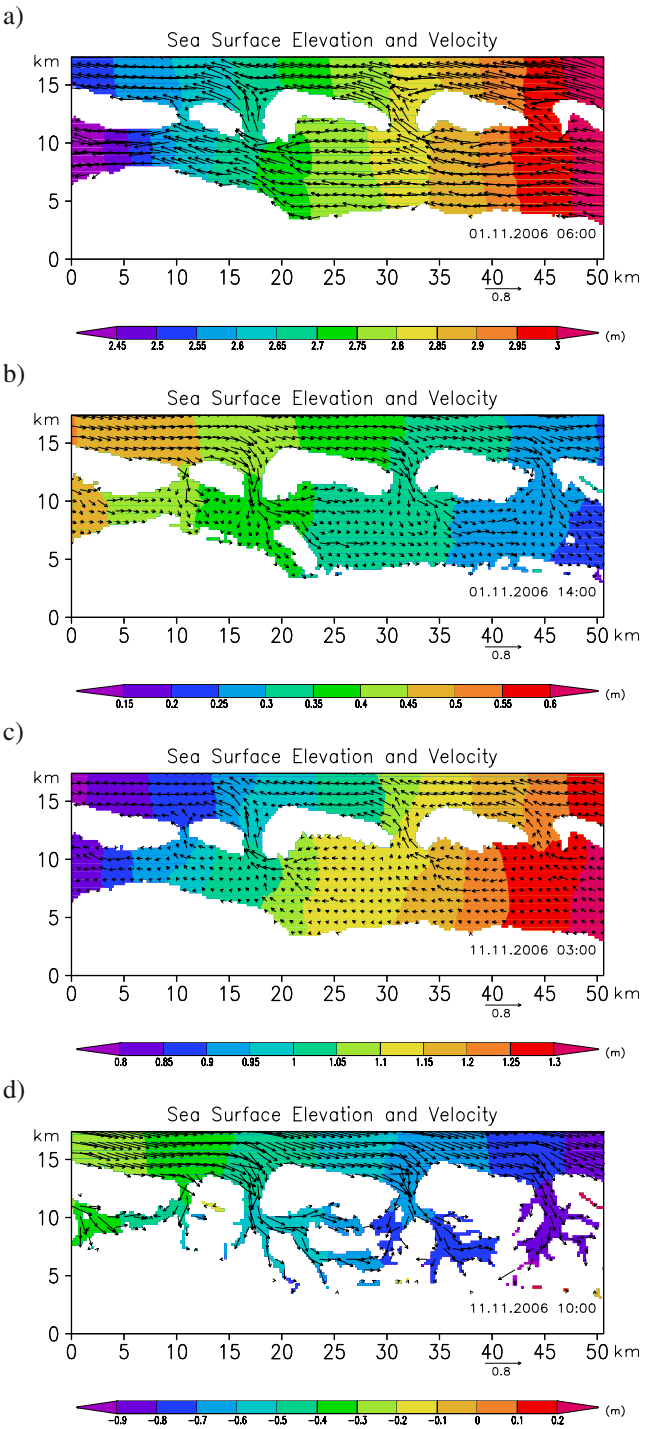

Fig. 4 Simulated surface velocities during ebb (**a** and **c**) and flood (**b** and **d**). **a** and **b** correspond to 1 November, **c** and **d** to 11 November. *Colors* illustrate gradients in sea level

lag (Fig. 6a). It becomes clear from Fig. 6b that the reason for the success of the model system in simulating storm surges is not only the Wadden Sea model but also the GBM, which realistically simulates the transition of sea level from the open ocean to the coast. In the GBM,

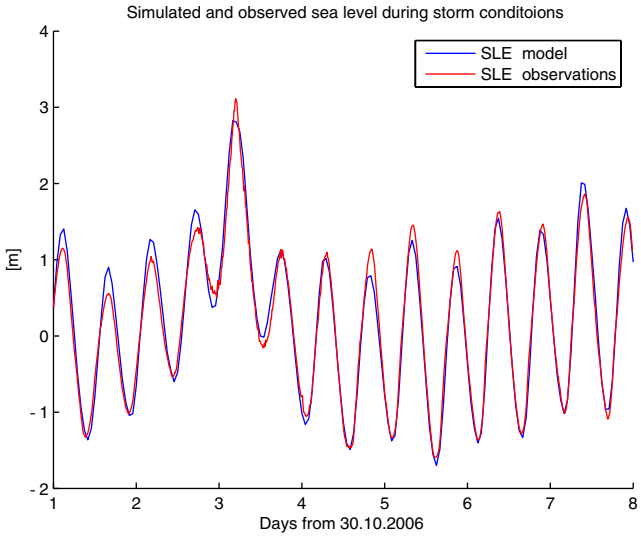

Fig. 5 Simulated (*blue line*) and observed (*red line*) sea level elevation at data station in Otzumer Balje (see Fig. 1 for the location) during storm conditions

amplitudes and phases differ substantially in the north–south direction, the slope ranging from ∼1 m/200 km during normal conditions to ∼2.5 m/200 km during storm Britta. The reason for extremely high water was the long duration of strong northwest wind (up to 156 km/h) working in parallel with the tides.

3 Empirical orthogonal function—analysis of simulations

3.1 Temporal variability

Statistical decomposition of time-space signals with the help of empirical orthogonal function (EOF) analysis facilitates the understanding of the most important spatial patterns and their temporal evolution (see, e. g., von Storch and Zwiers 1999). The latter are usually called principle components (PC). Sometimes, a direct link can be seen between the spatial (EOF) and PC patterns from one side and physical processes from the other side, which is not theoretically justified by the method. However, we will demonstrate that, in our particular case, as in many other cases, most of the statistical information has a high level of physical consistency (see also Stanev et al. 2007b).

The overall behavior of dynamics can be better understood if we analyze the complete dataset; therefore, we do not process each individual field one by one, but take sea level and two velocity components as one state vector. The advantage of this approach is that it

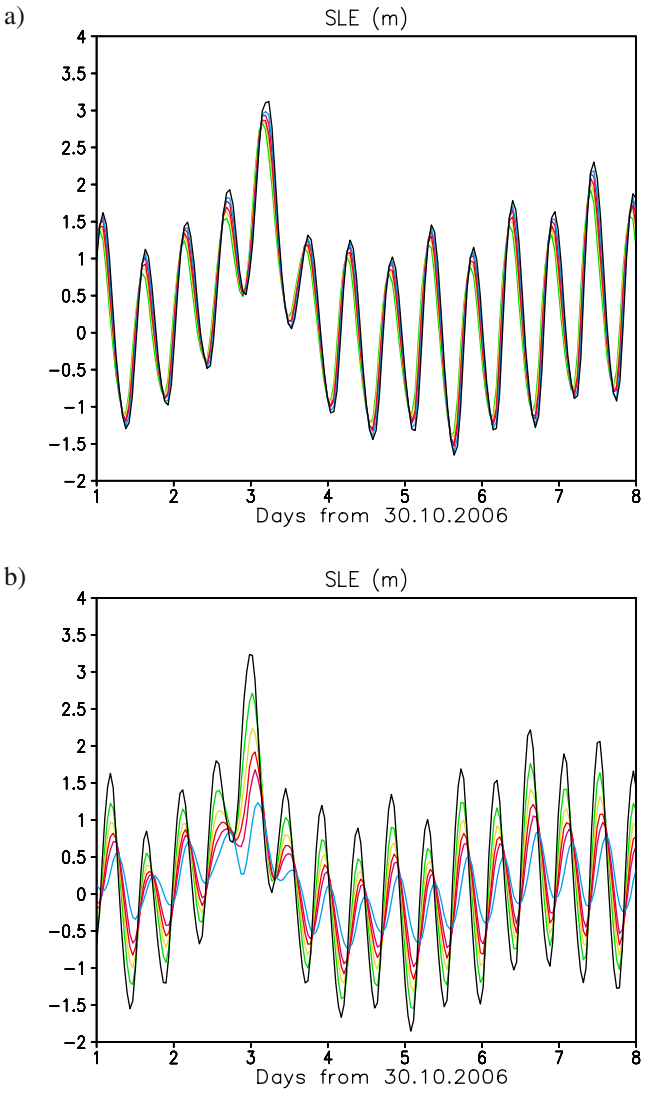

Fig. 6 **a** SLE along the northern boundary of the Wadden Sea model (locations are taken at equal distances of 12 km). The *black line* corresponds to the location just north of the WATT-data station in Otzumer Balje (Fig. 1). **b** SLE along the meridian passing through the WATT-data station in Otzumer Balje (locations are taken at equal distances of 25 km). The *thick black line* gives the course of sea level closest to the northern boundary of the Wadden Sea model. The *blue line* displays SLE closest to the northern boundary of the GBM

is coherent with procedures used in some data assimilation techniques. The disadvantage is that it might not clearly display some major physical characteristics of individual fields. To simplify the analysis and to avoid transformations from sigma into z-coordinate system, we analyze surface and bottom properties only. From the analyzed fields, we present here the statistical characteristics of sea level and surface currents.

From the period September–December, we chose two periods, which are characterized by calm weather

(18 September 2006–2 October 2006, hereafter "calm") and weather dominated by strong winds (1–14 December 2006, hereafter "windy", see Fig. 3). For these periods, we process the model data sampled with 60-min resolution. Furthermore, to ensure homogeneous datasets in "calm" and "windy," we exclude from the analysis locations that fall dry.

Another analysis has been performed for the whole period of integration using filtered model output. Filtering is performed with a diurnal time-window. This analysis is briefly called "no-tidal," although filtering retains in the analyzed data, along with the synoptic variability, longer-term variability associated with the spring–neap tidal cycle.

The percentage of variance explained by the first three oscillation modes in "calm" and "windy" cases (Table 1) demonstrates that the tidal signal (see also Fig. 7) is the strongest one. As the response of the shallow Wadden Sea to tidal forcing is relatively simple (Stanev et al. 2003, b), a very limited number of modes describes the total variance quite well.

A comparison between PC-1 (Fig. 7a) and the analyzed fields demonstrates that this component almost repeats the tidal oscillations of the sea level. PC-2 shows a phase shift of about a quarter tidal period relative to PC-1 and corresponds to velocity oscillations. This curve represents semidiurnal tidal oscillations modulated by spring–neap periodicity. The well-known asymmetry associated with the nonlinear response of tidal flats (Stanev et al. 2003) is seen in this signal: different times are needed to establish maximum flood or maximum ebb velocity (Fig. 8). In particular, longer time is needed for the currents to evolve from maximum ebb to maximum flood than for the inverse transformation (note that negative PC-2 corresponds to flood). This does not only support the theoretical results mentioned above, which have been mostly applied to tidal channels, but also demonstrates that the so called "ebb-dominance," or, according to the terminology of Friedrichs and Madsen (1992), "shorter-falling asymmetry," dominates the tidal response in this region as a whole.

PC-3 (Fig. 7c) represents ~6-hourly periodicity, which is associated with the maximum in current magnitude (twice per tidal period). This type of variability

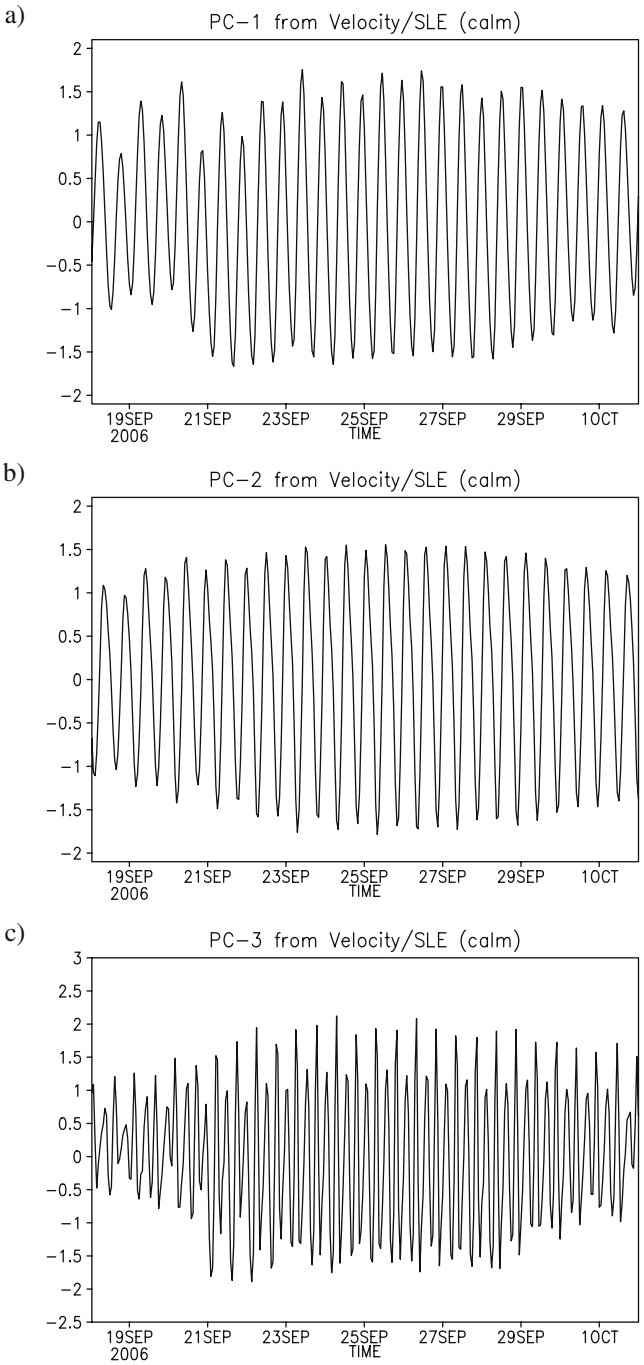

Fig. 7 The first three PCs in "calm" corresponding to dynamical variables (sea level and velocity) (**a**–**c**)

Table 1 Percentage of variance explained by the first three EOFs

Mode	Calm		Windy	
No	Dynamics	TKE	Dynamics	TKE
1	82.7	86.3	83.1	85.4
2	16.7	6.7	16.3	6.8
3	0.2	2.7	0.2	2.8
Sum	99.6	95.7	99.6	95.0

is similar to the type of variability detected in observations (Stanev et al. 2007b), namely, the two maxima are different (the one during flood is higher; see Fig. 8).

TKE has been analyzed separately from dynamic variables (sea level and velocity) as a single state vector. The major characteristics of the PCs of TKE is the quaterdiurnal periodicity (about 6 h), which is pronouncedly modulated by the spring–neap signal (Fig. 9). This is just an illustration that the level of TKE in the Wadden Sea is very sensitive to this important astronomical forcing. The second important characteristic of turbulence is the strong difference in the PC maxima during flood and ebb. This gives a clear support of earlier theories about asymmetric responses (Stanev et al. 2007b), which are enhanced during spring-tide. Comparison between the PC-1 of TKE and the sea level curve (not shown here) demonstrates that maximum amplitudes in TKE are reached at high water during spring tide. This result could provide an indication that, during this part of the tidal period, resuspended sediment and sediment eroded from the bottom (here, we assume that concentrations are expected to reach higher values if turbulence is stronger) is transported landwards. This could provide an explanation as to why tidal flats tend to accumulate sediment.

Comparison of the PCs during calm and windy weather shows that no remarkable differences can be identified (see also Table 1). This supports the idea that, in the Wadden Sea, tidal response is dominating, therefore, the corresponding curves from the "windy" period are not shown here. However, the model output from which frequencies higher than diurnal ones have been filtered out gives quite a different view on the temporal variability (Fig. 10). In this data set, the

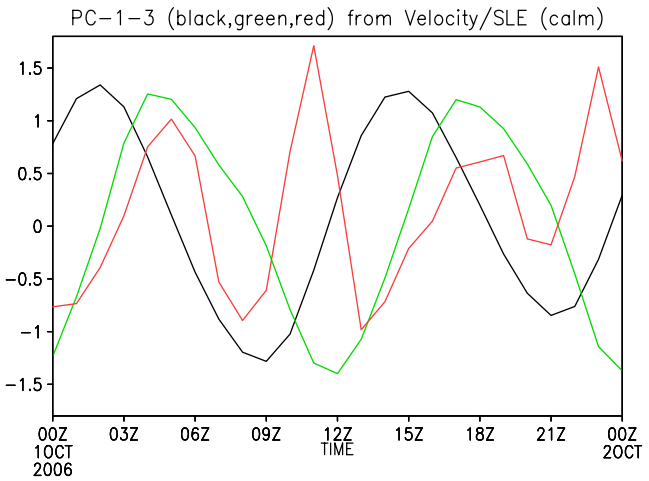

Fig. 8 Time-zoom in the first three PCs, PC-1 (*black*), PC-2 (*green*), and PC-3 (*yellow*) of sea level and velocity in "calm"

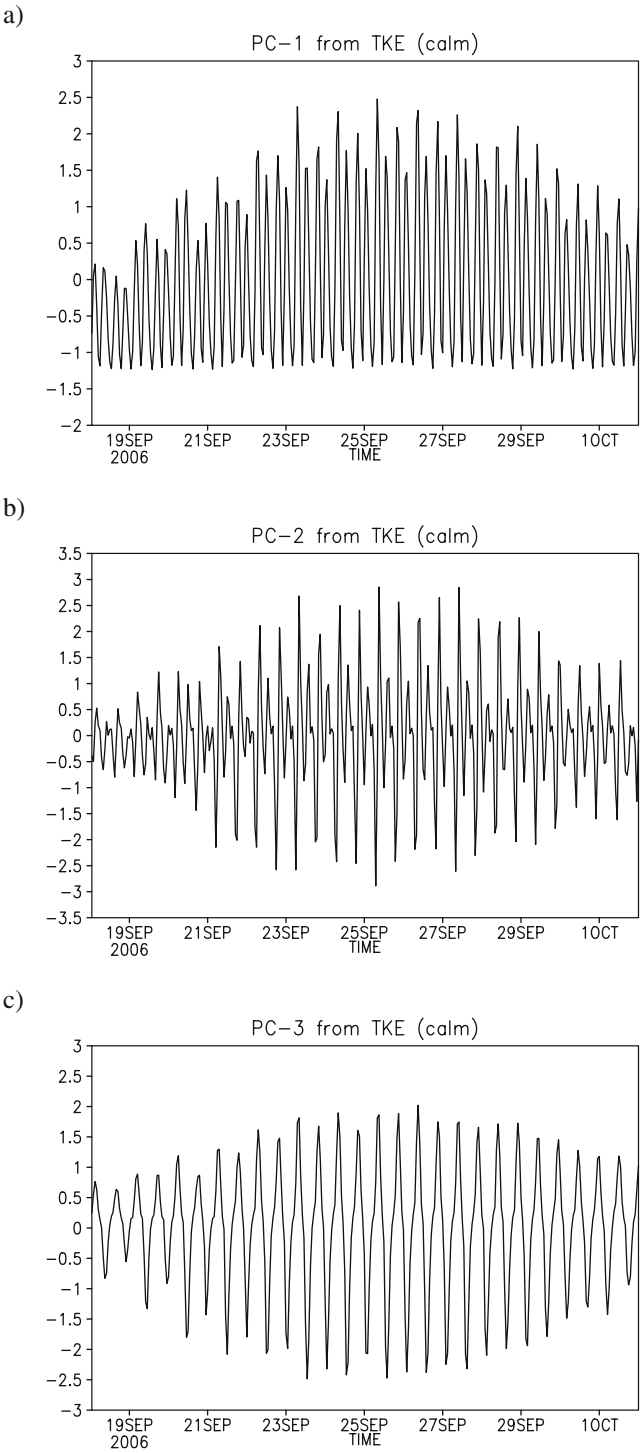

Fig. 9 The first three PCs in "calm" corresponding to TKE (**a**–**c**)

first three EOFs describe 76.3%, 11.0%, and 5.6% of the total variance (97.9% in total). PC-1 shows some correlation both with the course of SLE forcing (dashed red line in Fig. 10a) for some of the extreme events and wind magnitude (dashed blue line in Fig. 10a) for

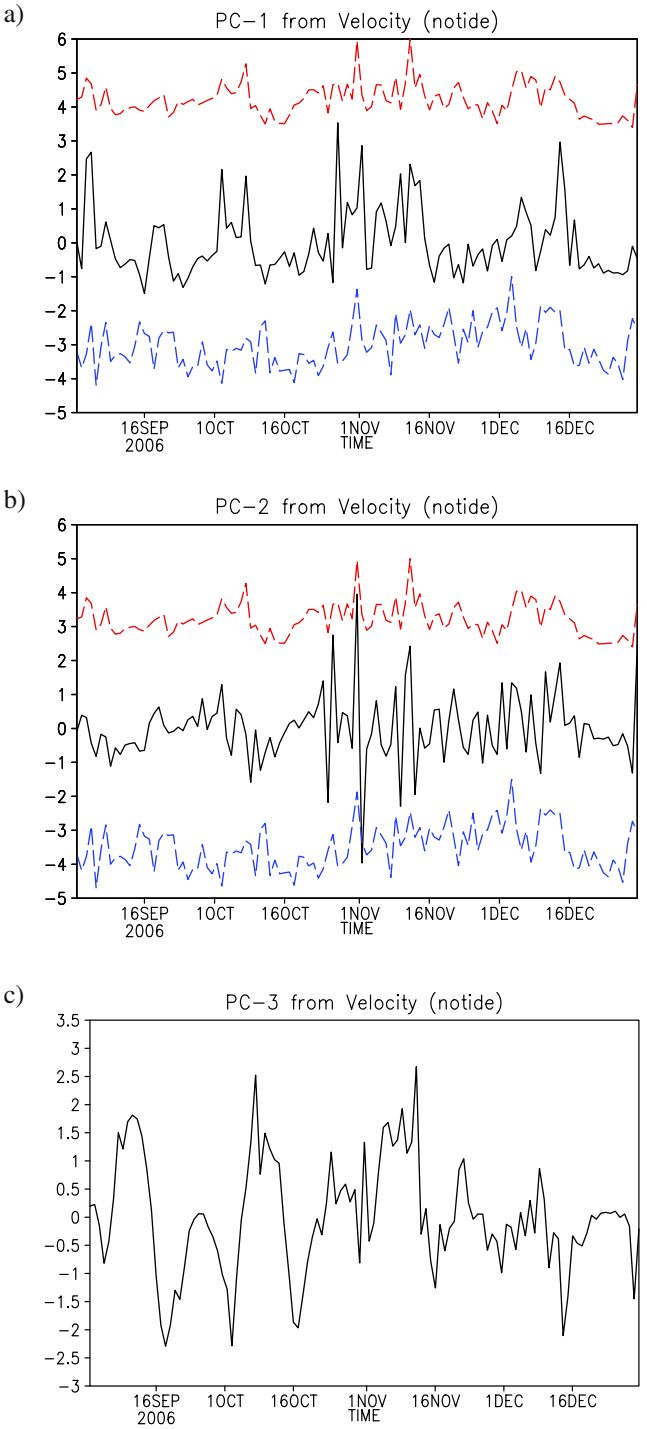

Fig. 10 The first three PCs in "no-tide" corresponding to dynamical variables (sea level and velocity). *Dashed lines* in **a** and **b** give the course of wind magnitude (*blue*) and sea level at the open boundary (*red*) scaled and shifted in order to enable comparison with the PCs

longer-term variability. PC-2 is dominated by extreme events (storm surge Britta), while PC-3 is modulated by spring–neap oscillations, particularly for the calmer first part of the analyzed period (see Fig. 3).

One comparison between Figs. 10 and 3 is worthy of discussion for its geophysical relevance. Wind speed maxima during storm surge Britta and during the "windy period" are comparable. However, the response of sea level in the coastal area is very different. Furthermore, the projections of these events on the PCs differ. While the extreme signal during the "windy period" is seen in PC-1 (Fig. 10a), there is just noise during this period in PC-2 (Fig. 10b). Obviously, the extreme wind did not last long enough and was rather variable during the "windy period." This signal is reduced significantly due to filtering with the diurnal time window (Fig. 10). Consequently, the ocean response in the model was weak even though the integration has been carried out with nonfiltered data.

3.2 Horizontal patterns

The first EOF in the "calm" period (Fig. 11a) is positive throughout the model area. This oscillation mode displays the vertical motion of the sea level caused by tides, which is unidirectional over the entire area. The east–west gradient illustrates the fact that the tidal range in this region increases from west to east. Tidal channels show a tidal range as high as the adjacent open-ocean areas north of them.

A parallel analysis of the entire data set including data in the regions reaching a dry state was also conducted. Results are not shown here because data series are not homogeneous (sea level is "frozen" in the model when the water column thickness reaches the minimum allowable value of 2 cm). Nevertheless, the two analyses demonstrate no big differences in the deep regions. In the regions undergoing drying and flooding, EOF-1 of the sea level follows the bottom topography (smallest variability in areas remaining dry for longer times) and, as it was the case for deep data only, has the same sign throughout the model area.

EOF-2 (Fig. 11b) shows an east–west propagation pattern and gives a measure of the phase difference between channels and the areas north of the barrier islands. The delay is approximately equal to the time needed for the tidal wave to cover the distance of about one barrier-island length (notice that we observe same colors, green in this case, in front of Spiekeroog and behind Langeoog islands).

From the horizontal pattern of EOF-3, it seems plausible that this mode corresponds to another known physical process, that is the east–west asymmetry of 6-h variability, which is enhanced during flood. Notice that, in this case, the response of the tidal channels is coherent with the processes north of the tidal inlets.

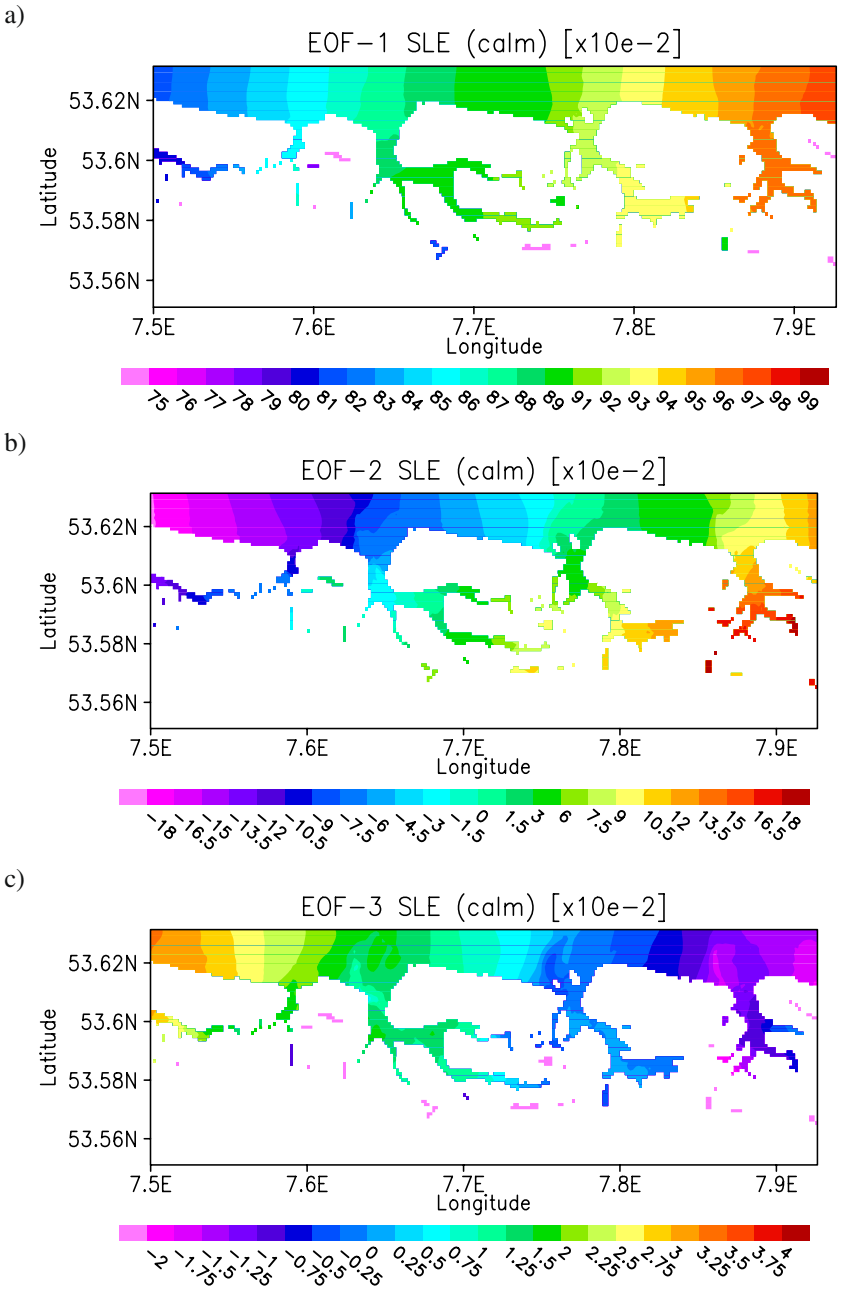

Fig. 11 The first three SLE EOFs in "calm" (**a**–**c**)

Furthermore, bearing in mind that (1) this variability pattern is dominated by 6-h oscillations and (2) that the analysis of the entire data set (deep area and area undergoing drying) shows inverse trends in the deep part and over the tidal flats, one could also conclude that this signal is indicative of the transformation of the tidal response in the Wadden Sea in a way that the ~6-hourly variability is coherent over the entire region of the tidal flats (see also Stanev et al. 2003).

EOF-1 of zonal surface velocity (Fig. 12a) displays an inverse correlation between the variability in tidal channels and the shallow area adjacent to the northern coasts of the barrier islands (the north-west tips of the barrier islands give the "origin" of the inverse to the tidal channels signal). Furthermore, a negative correlation is also observed between the area along the northern model boundary and the shallows north of the barrier islands. The latter structure is indicative of the rotational character of the tidal excursions north of the barrier islands. This type of oscillation is coherent with the vertical motion of sea level (see Fig. 7).

EOF-1 of meridional surface velocity (Fig. 12b) shows a pronounced anticorrelation between processes in the tidal channel Otzumer Balje (and, to a lesser extent, in the Accumer Ee) and the ones north of the islands of Spiekeroog and Langeoog (blue colors in

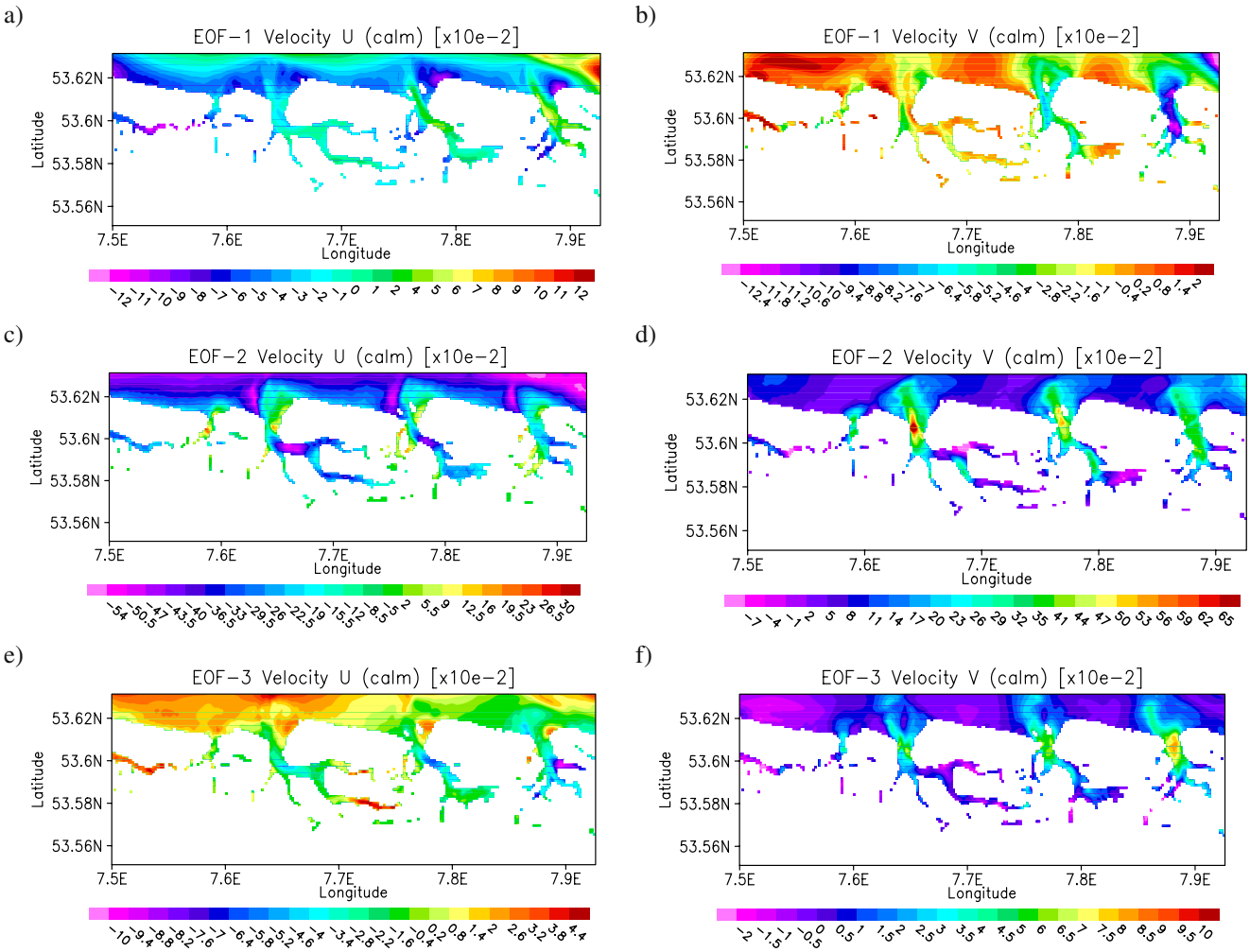

Fig. 12 The first three surface velocity EOFs in "calm", **a**, **c**, and **e**, U; **b**, **d**, and **f**, V

inlets and red colors north of the islands). A similar anticorrelation is observed between processes in tidal channels and tidal flats in the EOF analysis in which data in the areas undergoing drying are also processed (not shown here).

EOF-2 of the zonal and meridional surface velocities (Fig. 12c, d) displays some important characteristics of the dynamics of tidal channels. The inverse correlation (in particular, in u-EOF-2) enables us to identify the split of channels areas as flood- and ebb-dominated ones, which is also known from observations (Stanev et al. 2007b). The transformation of the v-signal along tidal channels (maxima and minima in Fig. 12d) gives a clear support of the theory (Stanev et al. 2007b) that tidal channels in the East Frisian Wadden Sea evolve from ebb-dominated (between barrier islands) to flood-dominated (in their shallowest extensions).

North of the barrier islands, an eastward "protrusion" of v-EOF-2 pattern is clearly seen, which is indicative of the export patterns from the tidal flats (from the western inlet to the eastern one).

The horizontal patterns of the 6-h variability (see Figs. 7c and 12e, f), which is mostly associated with currents magnitude, show quite different patterns for the two velocity components. While for the meridional transport the maximum variability is limited to the narrow area between neighboring islands (Fig. 12f), maximum variability of zonal transport is observed north of the barrier islands and in the zonal part of the channels. The latter is to be expected. However, what is not so trivial is the inverse correlation between u-patterns in different zonal sections of the channels, indicating a more complicated evolution of the tidal responses.

The horizontal patterns of TKE provide indirect information about the location of areas favorable to deposition and erosion. EOF-1 pattern, which is a unidirectional variability over the entire area (Fig. 13a),

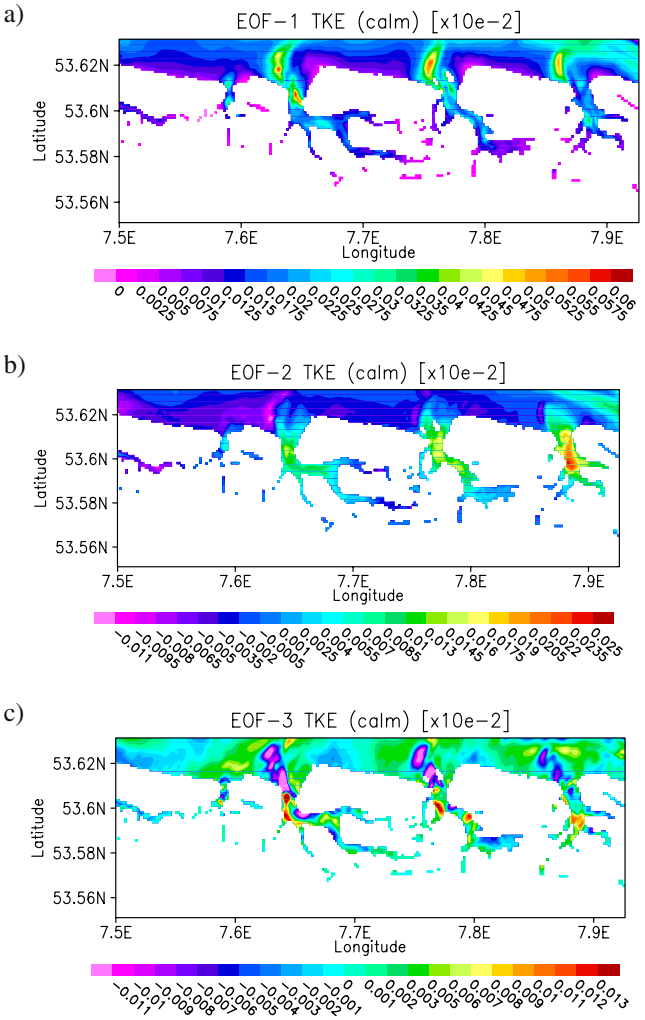

Fig. 13 The first three TKE EOFs in "calm" (**a**–**c**)

clearly demonstrates large differences in the magnitudes of oscillations in tidal channels and flat areas in front and behind the barrier islands. In addition to the well known asymmetries explaining tendencies of erosion and deposition in the Wadden Sea (Groen 1967; Postma 1982; Stanev et al. 2003b, 2007b), we see in the TKE-EOF-1 pattern different magnitudes in deep parts of the channels and their northern extensions from one side and in the remaining areas from the other side.

EOF-2 of TKE seems easier to interpret. This variability is strongly dominated by the neap–spring cycle, enhancing velocity magnitude along the channels (Fig. 13b). Eastern and westernmost areas of the open sea are inversely correlated, which demonstrates the sensitivity of TKE patterns to different tidal ranges in these zones. As for the TKE-EOF-3 (a very low-magnitude signal), the major horizontal characteristics are the opposing trends occurring in the channels north and south of the straits.

The analysis of temporal and spatial variability in the no-tide case is focused on transport characteristics because they give the clearest illustration of the response to extreme events. With respect to the sea-level characteristics, we will only mention that the response is relatively simple, as can be seen from Fig. 4, displaying a uniform in the north–south direction field. The EOF-1 (not shown here) shows a unidirectional change throughout the area.

EOF-1 of the zonal surface velocity component (Fig. 14a) has the same sign throughout most of the area. This could be explained by the adjustment of zonal circulation to winds with dominating zonal components. The strongest response (largest values of EOF-1) is observed in the open sea, which decreases with decreasing distance from the barrier islands. The EOF-1 and EOF-2 patterns of bottom velocity (not shown here) are similar to the ones in Fig. 14a, b, revealing that, in this area, there is no substantial change of dynamics with respect to the vertical coordinate.

Another interesting difference from tidal cases is observed in the no-tidal case: the zonal motion north of the islands displays some undulated patterns (Fig. 14a), which coincide well with irregularities in the bottom relief. This EOF structure is not observed in the case of tidal response.

In EOF-1 of meridional surface velocity (Fig. 14b), some pronounced differences from the "calm" period are obvious: the meridional transport in the channels Otzum Ee and Accum Balje is split into two: south-east of the tidal inlet, the correlation is positive with the oscillations along the coast of the western island. The blue-colored area (negative values) originating from the north-western tips of the barrier islands extends from north-west to south-east, thus cutting the area with positive values in two. In this way, a *quadropul-like pattern* is formed, which is characteristic for the regime of a two-way transport in the inlets driven by wind.

EOF-2 corresponding to longer-term variability of zonal surface velocity (Fig. 14c) is completely different from the one in the case of tidal forcing. The pattern north of the barrier islands (alternating positive and negative correlations) could indicate divergence and convergence in this component. As a whole, tidal flats and the areas north of the barrier islands are negatively correlated.

The propagation pattern associated with EOF-2 of meridional transport (Fig. 14d) is relatively simple and clear: the area north of the inlets is well defined and usually negatively correlated with the variability in most parts of the remaining open sea. This shows how the response to extreme events (storm Britta in this case) is horizontally structured.

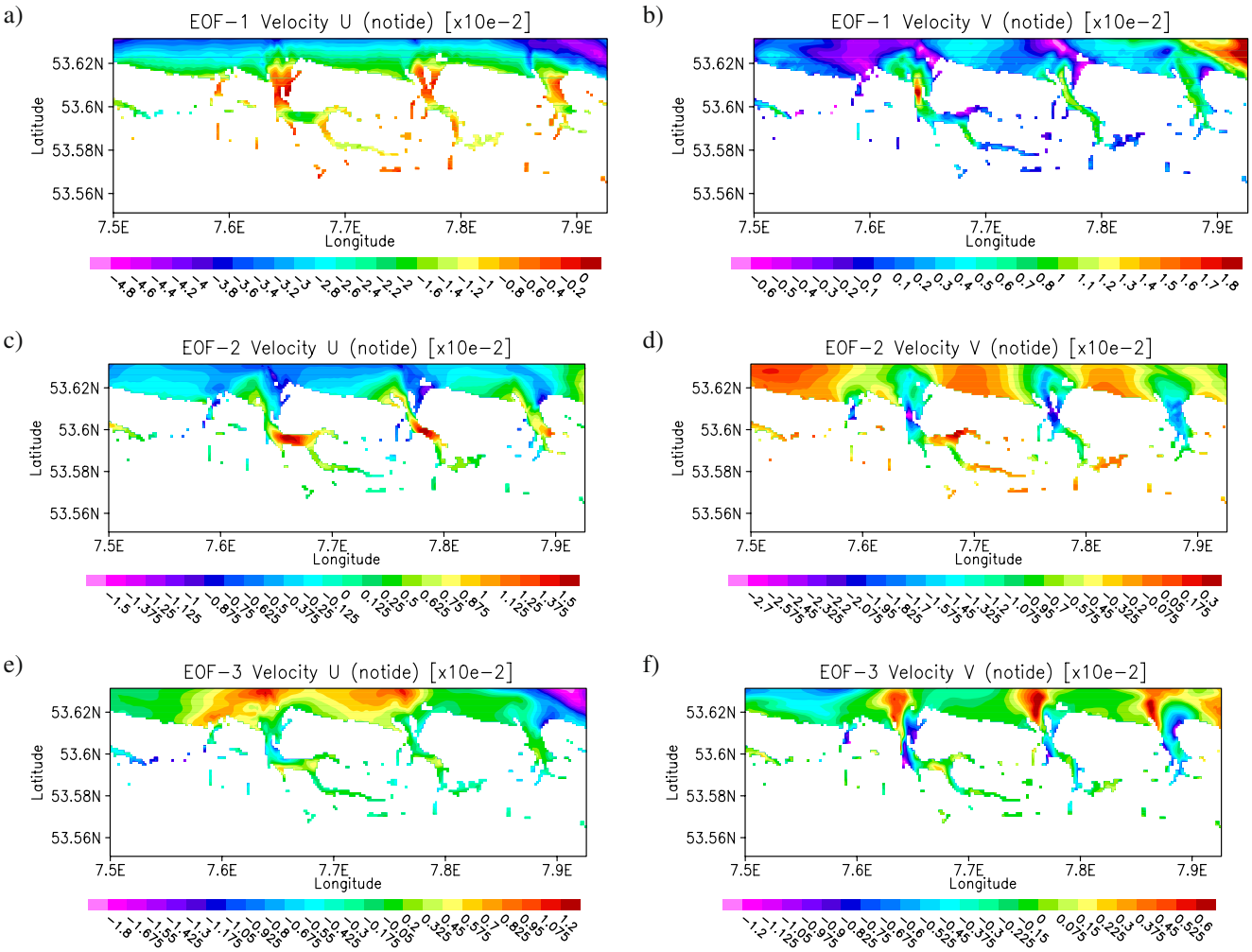

Fig. 14 The first three surface velocity EOFs in "notide", **a**, **c**, and **e**, U; **b**, **d**, and **f**, V

The two EOF-3 (Fig. 14e, f) reveal the response-patterns to the neap–spring cycle (see Fig. 10). Although this is a relatively weak signal compared to the one originating from extreme events, it is very well structured. The zonal component reflects an inverse correlation between western and central regions north of the barrier islands, while the meridional component pattern north of inlet is "divided" in two. This illustrates that evolution triggered by a neap–spring cycle might affect transport in the area of tidal deltas.

4 Statistical reconstructions

Provided that major processes could be well described by only a few EOFs, one might want to ask the question about the quality of statistical reconstruction and forecast. In order to address this issue, we use simulations during the "calm" period and the "windy" period. Then, using ten modes only, we reconstructed the simulations. Comparison between real (model output) and synthetic (reconstructed using limited amount of EOFs) data demonstrates that the mean error is about 0.03 sigma ("sigma" is the root mean square deviation) for the sea level and 0.12 and 0.19 sigma for u and v, correspondingly (Fig. 15). These are very small errors.

Motivated by the above results, we go one step further and ask the question: could a reconstruction (forecast) be done based on a limited amount of input information? In the Otzumer Balje (see Fig. 1b for the location), a continuously operating data station has been deployed (Staneva et al. 2008). The measured data (sea level temperature, salinity, and velocity at several levels) are available online and the use of these data for forecast purposes seems challenging. In the past few years, a similar data station operated by the *Gesellschaft zur Förderung der Kernenergie in Schiffbau und Schiffstechnik* Research Centre was

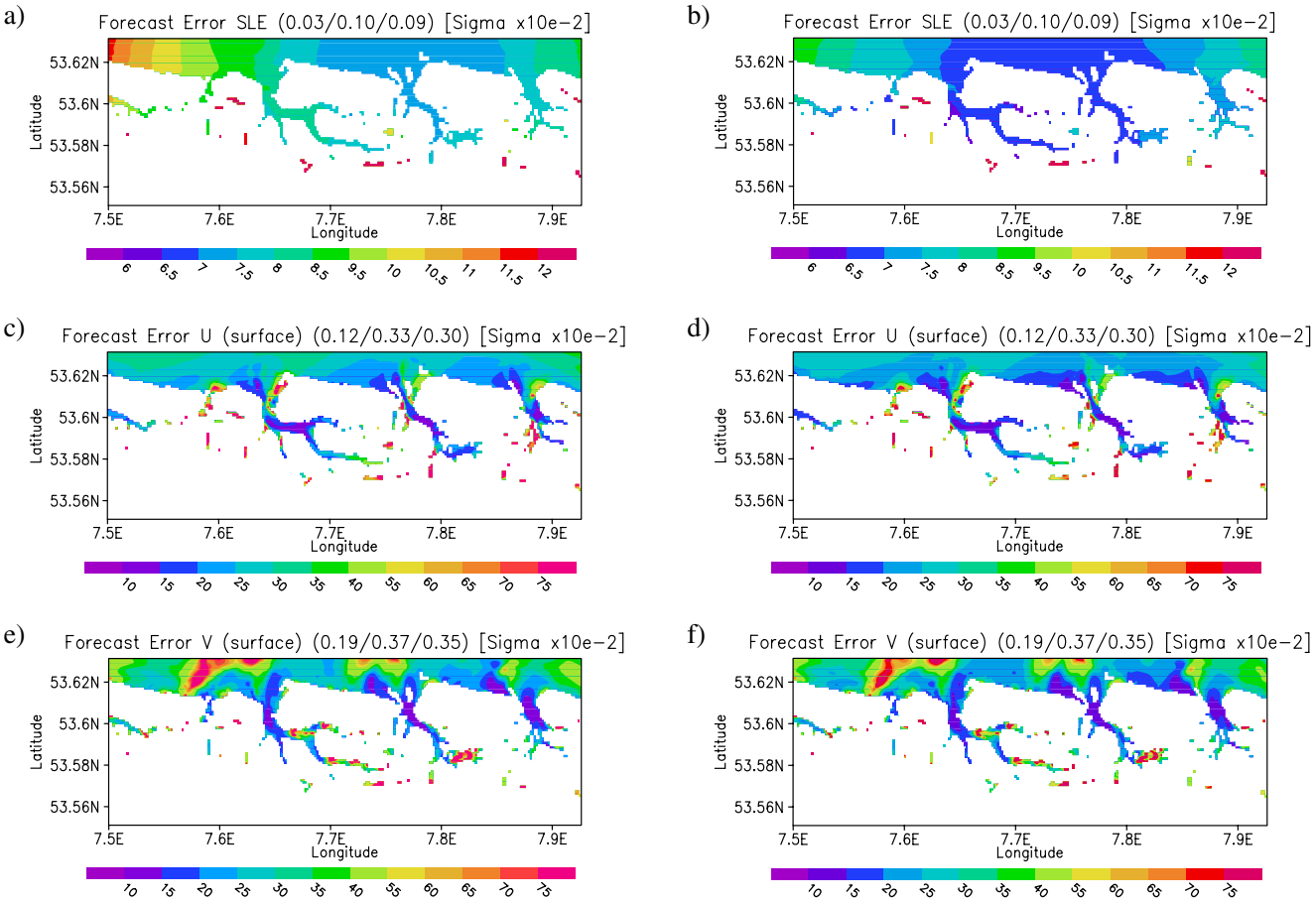

Fig. 15 Forecast error for sea level (**a**, **b**), u-surface-velocity (**c**, **d**), and v-surface-velocity (**e**, **f**). *Left column*: based on one data station, *right column*: based on two data stations. The heading of each plot contain the area mean values of errors of reconstruction, forecast using one data station, and forecast using two data stations

deployed in the Accumer Ee (square in Fig. 1b). The second question is: would it be possible using data from both stations to increase the quality of reconstructions, compared to the case of only a one-station statistical forecast?

Led by the two questions above, we take the model data only in the positions of data stations and construct by multivariate EOF analyses of extracted variables the PCs of "observations" (synthetic observations) for both periods (PC_{oc} and PC_{ow}). Indices "o," "c," and "w" stand for "observations," "calm," and "windy," respectively. For the forecast based on one data station (sea level and two velocity components at sea surface and bottom), we are able to calculate five PCs at most. For the forecast based on two data stations, ten PCs can be derived. We use the same amount of global domain PCs from the "calm" period (PC_{gc}, here, index "g" stands for "global") to "train" the forecast. Therefore, we apply a linear regression on PC_{oc} and PC_{gc} and obtain a set of linear parameters (L_c) to convert PCs of observations into PCs of the global domain. Finally, the forecast of the "windy period" (F_w) is calculated by:

$$F_w = \mathrm{EOF}_c \cdot L_c \cdot \mathrm{PC}_{ow} \quad (1)$$

For comparison, we also calculate a reconstruction of the "windy period" (R_w) from the first ten EOFs and PCs of the "windy period" by:

$$R_w = \mathrm{EOF}_w \cdot \mathrm{PC}_w \quad (2)$$

The root mean square forecast and reconstruction errors are calculated at each grid point and are shown as maps of percentage of standard deviation (Fig. 15). The heading of each plot shows the area mean values of errors of reconstruction, the forecast using one data station, and the forecast using two data stations. Obviously, the statistical forecast is worse than the reconstruction. However, taking into consideration the usual errors in observations, the results are encouraging.

Something unexpected from our reconstructions deserves to be mentioned here. The initial expectation

was that adding one more data stations would substantially increase the accuracy of the forecast. This, however, appeared not to be the case because the two data stations are very well correlated (see results in Section 3). Actually, not much new information is added by adding data from the second station. Additional reconstructions and forecasts based on different positions of data stations (not shown here) indicate that some improvement is still possible by optimizing the deployment of stations.

5 Conclusions

This paper presents a statistical analysis of numerical model simulations, which could be considered as a first step towards data assimilation of continuous observations in the Wadden Sea. This could have direct application when deciding about space reduction using EOFs. Some of the results support, in a more objective way, earlier results based on more limited analyses. In particular, temporal asymmetries due to specific hypsometric properties of tidal basins (ebb-dominance, or according to the terminology of Friedrichs and Madsen (1992) "shorter-falling asymmetry"), evolution of tidal signals along channels from ebb dominated between the barrier islands to flood dominated in their shallow extensions (Stanev et al. 2007b) are captured well by the statistical analyses and present fundamental temporal and spatial variability patterns for this area. We demonstrated that the coupled model system and its regional setup are quite successful in simulating not only tidally driven circulation, but also extreme events such as the storm surge Britta on 1. November 2006.

Parallel statistical analysis of circulation and turbulence supports our earlier studies. It was demonstrated that the level of TKE in the Wadden Sea is very sensitive to the spring–neap tidal forcing. More specifically, the large differences in the maxima in PC during flood and ebb are enhanced during spring-tide. Thus, the higher level of turbulence could result in an increase of sediment concentrations during flood. Consequently, increased sediment concentration leads to an enhancement of landward sediment transport, which could provide an explanation as to why tidal flats tend to accumulate sediment.

It has been shown that, without losing much detail, the information about circulation is easily "compressible" using several EOF modes only. Furthermore, it appeared possible to relatively correctly reconstruct and statistically forecast spatial dynamics using local measurements only. This allows us to conclude that the proposed method could be used as a reliable tool for simple and rapid estimates of the sea state in the vicinity of the continuously operating data station in the Spiekeroog Inlet. These conclusions hold only for the tidal part in the small domain. The nontidal part is much more complicated and further research is needed, involving data assimilation practices in order to clarify details about predictability of currents in the Wadden Sea, given their smaller spatial and temporal correlation scales and their strong interaction with the sea bed behind the islands. For the entire German Bight, however, our preliminary analyses on simulations with the GBM show that the reconstruction of nontidal dynamics is also reasonably good, though errors are higher than in the small area addressed in the present study.

Our belief is that the results presented are relevant to other similar cases of coastal dynamics and could motivate wider application of the techniques used here beyond the currently studied area.

Acknowledgements We acknowledge the financial support of *Deutsche Forschungsgemeinschaft* through the research project "BioGeoChemistry of Tidal Flats" and the EC-funded IP ECOOP.

References

Burchard H, Bolding K (2002) GETM—a general estuarine transport model. Scientific Documentation, No EUR 20253 EN, European Commission, printed in Italy, 157 pp

Burchard H, Flöser G, Staneva JV, Badewien TH, Riethmüller R (2008) Impact of density gradients on net sediment transport into the Wadden Sea. J Phys Oceanogr 38(3):566–587

Dick SK, Eckhard K, Müller-Navarra SH, Klein H, Komo H (2001) The operational circulation model of BSH (BSHcmod)—Model description and validation. Ber Bundesamtes Seeschiffahrt Hydrogr 29:49

Dick SK, Sötje K (1990) Ein operationelles Ölausbreitungsmodell für die deutsche Bucht. Dt Hydrogr Zeitschrift Ergänzungsheft Reihe A 16:243–254

Friedrichs CT, Madsen OS (1992) Nonlinear diffusion of the tidal signal in frictionally dominated embayments. J Geophys Res 97:5637–5650

Gayer GS, Pleskachevsky DA, Rosenthal W (2006) Numerical modeling of suspended matter transport in the North Sea. Ocean Dyn 56(1):62–77

Groen P (1967) On the residual transport of suspended matter by an alternating tidal current. Neth J Sea Res 3(1967):564–574

Postma H (1982) Hydrography of the Wadden sea: movements and properties of water and particulate matter. In: Postma H (Ed) Final report on hydrography of the Wadden Sea, Working Group Report 2. Balkema, Rotterdam, p 76

Reinke E, Huisinga W, Brechters C, Maarfeld S, Honczek S, Beekmann R, Rosendahl E, Buss M, Tapper D (2000) Nährstoffeinträge in die Nordsee. Phosphor- und Stickstofffrachten aus Sielen und Schöpfwerken Ostfrieslands in den Jahren 1997–1999, Report of Niedersächsischer Landesbetrieb für Wasserwirtschaft, Küsten- und Naturschutz, p 80

Santamarina Cuneo P, Flemming B (2000) Quantifying the concentration and flux of suspended particulate matter through a tidal inlet of the East Frisian Wadden Sea by acoustic Doppler current profiling. In: Flemming BW, Delafontaine MT, Liebezeit G (Eds) Muddy coast dynamics and resource management. Elsevier Science, Amsterdam, pp 39–52

Stanev EV, Brink-Spalink G, Wolff J-O (2007a) Sediment dynamics in tidally dominated environments controlled by transport and turbulence: a case study for the East Frisian Wadden Sea. J Geophys Res 112:C04018. doi:10.1029/2005JC003045

Stanev EV, Flemming B, Bartholomä A, Staneva J, Wolff J-O (2007b) Vertical circulation in shallow tidal inlets and back barrier basins. Cont Shelf Res 27(6):798–831

Stanev EV, Flöser G, Wolff J-O (2003a) Dynamical control on water exchanges between tidal basins and the open ocean. A case study for the East Frisian Wadden Sea. Ocean Dyn 53:146–165

Stanev EV, Wolff J-O, Brink-Spalink G (2006) On the sensitivity of sedimentary system in the East Frisian Wadden Sea to sea-level rise and magnitude of wind waves. Ocean Dyn 56(3–4):266–283

Stanev EV, Wolff J-O, Burchard H, Bolding K, Flöser G (2003b) On the Circulation in the East Frisian Wadden Sea: numerical modeling and data analysis. Ocean Dyn 53:27–51

Staneva J, Stanev EV, Wolff J-O, Badewien TH, Reuter R, Flemming B, Bartholomä A, Bolding K (2008) Hydrodynamics and sediment dynamics in the German Bight. A focus on observations and numerical modelling in the East Frisian Wadden Sea. Cont Shelf Res. doi:10.1016/j.csr.2008.01.006

von Storch H, Zwiers FW (1999) Statistical analysis in climate research. Cambridge University Press, Cambridge, 494 pp